DESIGNING AND MODELLING OF AN MIC FOR HYBRID POWER CHARGER SYSTEM

PG SCHOLAR **THASNI S HABEEB**

ASSISTANT PROFESSOR **RAJA SRINIVASAN.S.P , M.E**

DEPARTMENT OF ELECTRICAL AND ELECTRONICS

SATYAM COLLEGE OF ENGINEERING AND TECHONOLOGY

Abstract—**The objective of this paper is to propose the development of a multi-input dc-dc converter (MIC) family which is composed of isolated and/or non-isolated dc-dc converters. By analyzing five basic isolated dc-dc converters, four isolated pulsating voltage source cells (I-PVSCs) and three isolated pulsating current source cells (I-PCSCs) are generated. Moreover, a semi-isolated multi-input converter (S-MIC) for hybrid PV/wind power charger system which can simplify the power system, reduce the cost, deliver continuous power and overcome high voltage-transfer-ratio problems is proposed. In this paper, the operational principle of the proposed S-MIC is explained, the small-signal ac model is derived and the controller design is developed. Computer simulations and experimental results are presented to verify the accuracy of the proposed small signal ac model and the performance of the proposed S-MIC.**

Index Terms—**Maximum power point tracking (MPPT), multi- input converter (MIC), renewable energy systems, modelling, and hybrid power integration.**

I. INTRODUCTION

NOWADAYS, renewable energy sources such as solar panels or wind turbines have been developed rapidly [1], [2]. However, because of their intermittent feature, different types of renewable energy sources should be integrated together in order to deliver less fluctuated and more reliable energy to the load [3], [4].

Generally, various sources can be connected in parallel at the load through an intermediate power converter to draw the maximum power and to increase the power reliability. However, in order to increase the flexibility of power expansion and the utilization of the power converter, different types of multi-input dc-dc converter (MIC) have been proposed [5]-[19].

The MIC can deliver power from different energy sources to the load simultaneously or individually. A systematic approach to develop the circuit topologies of the MIC had been proposed [20]. In [20], the concept of pulsating source cell (PSC), including pulsating voltage source cell (PVSC) and pulsating current source cell (PCSC), was first proposed and rules of connecting them with other dc-dc converters were established. However, in the previously published paper, the authors   only focus their efforts on the six basic non-isolated converters, which are buck, boost, buck-boost, Ćuk, SEPIC, and Zeta converters. For some applications with the need of high voltage-transfer-ratio or electricity isolation, the isolated power converter should be considered. Therefore, the synthesis of isolated MICs with a concise and systematic approach should be developed.

To synthesize the MIC with isolation property, the isolated PSC (I-PSC) needs to be generated in advance. The developed I-PSCs in this paper and the previously proposed PSCs in [17,20] can be integrated with either isolated or non-isolated converters to synthesize different types of MICs. Eventually, the

synthesized MIC can be further divided into three categories: Non-isolated MIC (N-MIC), Isolated MIC (I-MIC) and Semi-isolated MIC (S-MIC) which will form the whole MIC family. The N-MIC has no isolated transformer within the converter while each energy source of the I-MIC is electrically isolated to the load. For the S-MIC, only some of the energy sources are isolated to the load.

For the hybrid PV/wind power charger system application, since the output voltage of the battery and PV module are usually quite low and the rectified output voltage of the small-scale wind turbine might be much higher, the N-MIC might encounters some implementation difficulties due to the high voltage-transfer-ratio. Therefore, in this paper an S-MIC consists of a forward-type isolated PVSC (I-PVSC) and a buck-boost prime converter is proposed for the hybrid PV/wind power charger system to realize the maximum power point tracking (MPPT) function for each PV/wind source.

The MIC has several advantages such as providing simple circuit topology, centralized control and low manufacturing cost and size. However, it also contains multiple interacting variables. Therefore, in order to increase the dynamic response and stability of the MIC, the small-signal analysis of the MIC is necessary. Moreover, due to the cross-coupling nature of the MIC, the controller design is not as straightforward as the controller design in a single-input-single-output system. The control loop needs to be decoupled in order to separately design the closed-loop controllers. Many literatures have been found focusing on the modeling and control of a MIC [21]-[25]. For example, a two-loop control strategy for a buck-type PVSC SEPIC prime converter has been proposed in [21], with the small signal ac model developed for dc battery sources and a dc

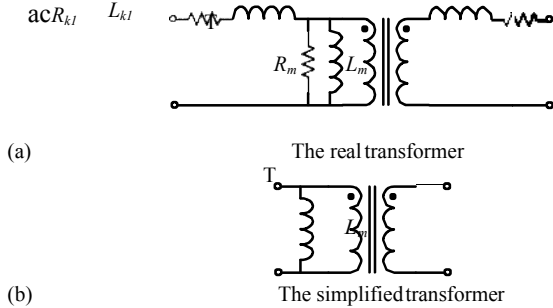load. The control strategy, power management, small signal ac

(a)   The real transformer

(b)   The simplified transformer

Fig. 1. Transformer equivalent circuit models.

(a)   The full-bridge type T

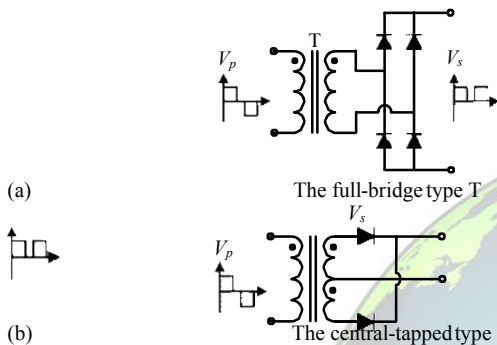(b)   The central-tapped type

Fig. 2. Different types of rectifier circuits for transformer secondary side.

model and decoupling network for an integrated three-port converter has been proposed in [23]. However, among these papers, the formation of different circuit topologies was not explained and their algebraic pole-zero form models have not been derived.

In this paper, the I-PSCs based on the operation principle of the isolated dc-dc converters are developed, the complete circuit topologies of N-MIC, I-MIC and S-MIC are obtained, the operational principle of the proposed S-MIC for hybrid PV/wind power charger system is explained, the small-signal ac model is derived, and the controller design is presented. Computer simulations and prototype circuit experimental results are presented to verify the accuracy of the small-signal ac model and the performance of the proposed S-MIC.

II.   THE ISOLATED PULSATING SOURCE CELLS

As the PVSC and the PCSC are generated from the six basic PWM converters [20], the I-PVSC and I-PCSC should be generated from basic isolated dc-dc converters, too. Basically, the circuit topologies for isolated dc-dc converters can be categorized as: flyback, forward, half-bridge, full-bridge, and push-pull. For an isolated dc-dc converter, the transformer plays the most important role in the circuit topology. Before the I-PVSC and I-PCSC can be developed, the transformer model need to be determined in advanced.

A commonly used real transformer circuit model is shown in Fig. 1 (a) which consists of an ideal transformer and other parasitic components, such as the winding resistance, R_{k1} and R_{k2}, the leakage inductance, L_{k1} and L_{k2}, the magnetizing inductance, L_m, and the magnetizing resistance, R_m. However, except for the L_m, the $R_{k1}, R_{k2}, L_{k1}, L_{k2}$, and the R_m do not involve

in the operation principle of the isolated dc-dc converter. They only affect the efficiency of the transformer. Consequently, the simplified transformer circuit model used in this paper only consists of an ideal transformer and a magnetizing inductor as shown in Fig. 1 (b). Furthermore, the L_m will not affect the operation principle of the half-bridge, full-bridge, and push-pull dc-dc converter, and it can be further neglected.

Besides the transformer circuit mode, different types of rectifier circuit topologies can be used at the secondary side of the transformer to provide the desired DC output. There are mainly two types of rectifiers available: the full-bridge type and the central-tapped one as shown in Fig. 2 (a) and (b), respectively. The full bridge rectifier needs four diodes but each diode has lower voltage stress. Besides, the realization of the transformer is easy and there is no secondary winging imbalance problem. Therefore, the full-bridge type rectifier is selected in this paper although the central-tapped type one can achieve the same function.

In the following, different types of I-PVSCs and I-PCSCs will be developed based on the above mentioned basic isolated PWM converter with simplified transformer circuit model and full-bridge type secondary rectifier.

A. Flyback

The circuit topology of a flyback converter is shown in Fig. 3 (a) with the input portion (IP) and output portion (OP) marked. Since the flyback converter uses the magnetizing inductor of the transformer as the energy storage component, a high frequency pulsating current will flow out the second winding of transformer. Eventually, the flyback-type I-PCSC can be defined and showed in Fig. 3 (b).

B. Forward

A forward converter circuit topology with the reset winding is shown in Fig. 4 (a) with the IP and the OP marked. When the power switch is turned on, the input voltage will be forwarded to the secondary winding of the transformer. During the turn-off stage, the rectifier diode D_1 will prevent the reverse power flow and the reset winding will demagnetize the transformer via the input voltage source. To form an I-PVSC with a pulsating voltage train, the parallel diode D_2 needs to be included to provide a current path for other sources. Therefore, the forward-type I-PVSC is obtained and shown in Fig. 4(b).

C. Push-Pull

The push-pull converter can be further classified as a voltage-fed converter or a current-fed one as shown in Fig. 5 (a) and (b), respectively. In Fig. 5 (a), the power switches S_1 and S_2 will generate an AC pulse-train voltage on the secondary side of the transformer while the rectifier diodes $D_1 \sim D_4$ transform the output voltage into a DC pulsating voltage source. Therefore, the voltage-fed push-pull-type I-PVSC can be obtained and shown in Fig. 6 (a).

Similarly, a pulsating current source can be obtained at the output terminals of the current-fed push-pull converter beyond the rectifier diodes. Eventually, the push-pull-type I-PCSC can be obtained as shown in Fig. 6 (b).
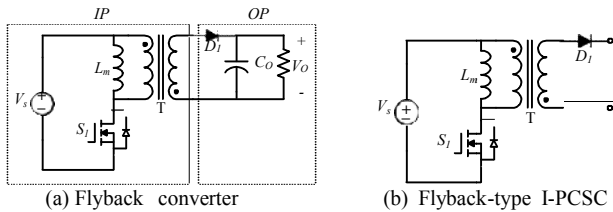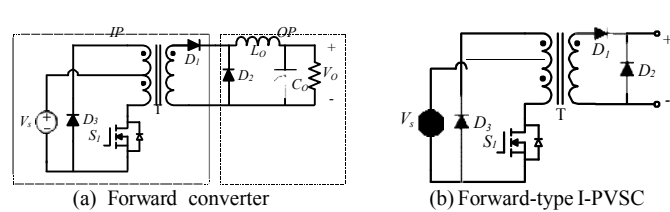
(a) Flyback converter   (b) Flyback-type I-PCSC
Fig. 3. Flyback converter and its developed I-PCSC.

(a) Forward converter   (b) Forward-type I-PVSC
Fig. 4. Forward converter and its developed I-PVSC.
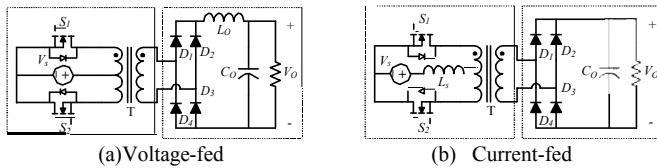
(a)Voltage-fed   (b) Current-fed
Fig. 5. Push-pull converters with different input sources.
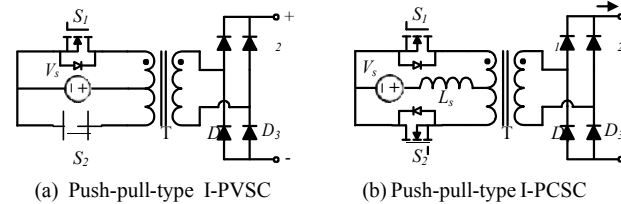
(a) Push-pull-type I-PVSC   (b) Push-pull-type I-PCSC
Fig. 6. Different push-pull-type I-PSCs.
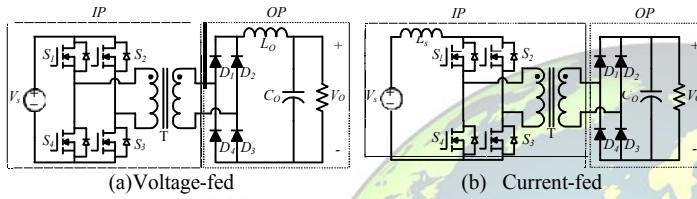
(a)Voltage-fed   (b) Current-fed
Fig. 7. Full-bridge converters with different input sources.

(a) Full-bridge-type I-PVSC   (b) Full-bridge-type I-PCSC
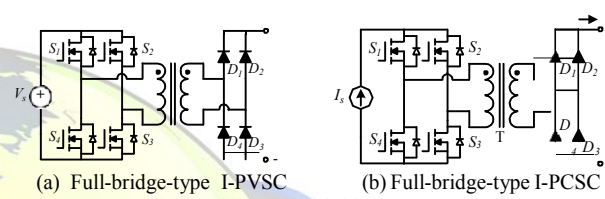Fig. 8. Different full-bridge-type I-PSCs.

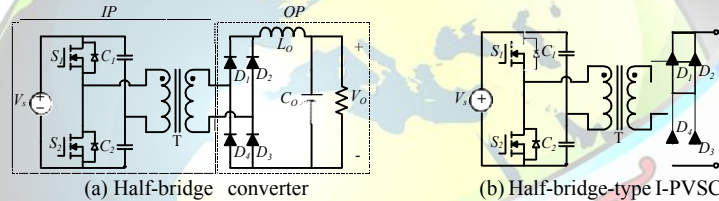(a) Half-bridge converter   (b) Half-bridge-type I-PVSC
Fig. 9. Half-bridge converter and its developed I-PVSC.

D. Full-Bridge

Full-bridge converters are also found to have both the voltage-fed type and the current-fed type. Circuit topologies of them with IP and OP marked are shown in Fig. 7. The operation principle of the full-bridge converter is similar to the one of the push-pull converter except that four switches are needed and only one primary winding of the transformer is required.

By following the development methodology of the push-pull-type I-PVSC or I-PCSC, the full-bridge-type I-PVSC or I-PCSC are illustrated in Fig. 8 (a) and (b), respectively.

E. Half-Bridge

The half-bridge converter needs two series-connected capacitors to form a voltage source. Therefore, it is always a voltage-fed converter. To form a current-fed half-bridge converter, an auxiliary circuit is needed [26]. However, this attempt is beyond the scope of the basic isolated converter and is not i Fig. 9 (a) shows the circuit topology of the half-bridge converter with IP and OP marked. The operation of the half-bridge converter is similar to the one of the voltage-fed full-bridge converter. Hence, the half-bridge-type I-PVSC can be obtained as shown in Fig. 9 (b).

By inserting the newly developed I-PVSCs/I-PCSCs or the PVSCs/PCSCs, proposed in [20], into different types of non-isolated or isolated dc-dc converters, different types of MICs can be obtained. Based on the isolation condition

between the input sources and the output load, the whole MIC family should include three series: N-MIC, S-MIC and I-MIC. The N-MIC series had been well-developed in [20]. The S-MIC can be synthesized by inserting the I-PVSC or I-PCSC into the non-isolated prime converter or by inserting the PVSC or PCSC into the isolated prime converter. In the former case, the I-PVSC or I-PCSC can be inserted into the energy buffer portion (EBP) or the OP of the non-isolated prime converter. But, in the latter case, the PVSC or the PCSC can be only connected to the OP of the isolated prime converter. The I-MIC can be synthesized by inserting the I-PVSC or I-PCSC into the isolated prime converter. Because the isolated prime converter only has the OP for the I-PVSC or I-PCSC to insert in, the member number of I-MIC series is relatively smaller. In this paper, the synthetic circuit topologies of the S-MIC series are list in Table I and Table II, while those ones for the I-MIC series are listed in Table III. In those tables, instead of circuit diagrams, numbers are adopted to represent different topologies. The same number in different Tables indicates the same circuit topology and those PSC which cannot find a suitable portion to synthesize a MIC will be mark as not available (*N/A*). The quasi-MICs with inserted PSC that cannot deliver power to the load individually are marked by asterisks. It should be mentioned that the developed MICs in this paper can be expanded to more than two input voltage sources.

TABLE I

THE SYNTHETIC CIRCUIT TOPOLOGIES OF THE S-MIC SERIES WITH ISOLATED PRIME CONVERTERS.

PSC \ PC		FR	FL	VF-PP	CF-PP	VF-FB	CF-FB	VF-HF
PVSC	Buck-type	1	*N/A*	2	*N/A*	3	*N/A*	4
	Ćuk-type	5	*N/A*	7	*N/A*	7	*N/A*	8
	Zeta-type	9	*N/A*	10	*N/A*	11	*N/A*	12
PCSC	Boost-type	*N/A*	13	*N/A*	14	*N/A*	15	*N/A*
	BB-type	*N/A*	16	*N/A*	17	*N/A*	18	*N/A*
	SEPIC-type	*N/A*	19	*N/A*	20	*N/A*	21	*N/A*
PC: Prime Converter, PSC: Pulsating Source Cell, FR: Forward, FL: Flyback, PP: Push-Pull, FB: Full-Bridge, HB: Half-Bridge, VF: Voltage-Feed, CF: Current-Feed, BB: Buck-Boost								

TABLE II

THE SYNTHETIC CIRCUIT TOPOLOGIES OF THE S-MIC SERIES WITH NON-ISOLATED PRIME CONVERTERS.

PSC \ PC		Buck	Boost	BB	Ćuk	Zeta	SEPIC
I-PVSC	FR-type	1	*N/A*	22	5	9, 23	24
	VF-PP-type	2	*N/A*	25	6	10, 26	27
	VF-FB-type	3	*N/A*	28	7	11, 29	30
	VF-HF-type	4	*N/A*	31	8	12, 32	33
I-PCSC	FL-type	*N/A*	13	16	34*	35*	19, 36*
	CF-PP-type	*N/A*	14	17	37*	38*	20, 39*
	CF-FB-type	*N/A*	15	18	40*	41*	21, 42*
PC: Prime Converter, PSC: Pulsating Source Cell, FR: Forward, FL: Flyback, PP: Push-Pull, FB: Full-Bridge, HB: Half-Bridge, VF: Voltage-Feed, CF: Current-Feed, BB: Buck-Boost							

TABLE III

THE SYNTHETIC CIRCUIT TOPOLOGIES OF THE I-MIC SERIES.

PSC \ PC		FR	FL	VF-PP	CF-PP	VF-FB	CF-FB	VF-HF
I-PVSC	FR-type	43	*N/A*	44	*N/A*	45	*N/A*	46
	VF-PP-type	44	*N/A*	47	*N/A*	48	*N/A*	49
	VF-FB-type	45	*N/A*	48	*N/A*	50	*N/A*	51
	VF-HF-type	46	*N/A*	49	*N/A*	51	*N/A*	52
I-PCSC	FL-type	*N/A*	53	*N/A*	54	*N/A*	55	*N/A*
	CF-PP-type	*N/A*	54	*N/A*	56	*N/A*	57	*N/A*
	CF-FB-type	*N/A*	55	*N/A*	57	*N/A*	58	*N/A*
PC: Prime Converter, PSC: Pulsating Source Cell, FR: Forward, FL: Flyback, PP: Push-Pull, FB: Full-Bridge, HB: Half-Bridge, VF: Voltage-Feed, CF: Current-Feed								

For the hybrid PV/wind power charger system application, since the output voltage of the battery and PV module are usually quite low and the rectified output voltage of a wind turbine might be much higher, an S-MIC composed of a portion for high step down and a portion for both step up and step down will be a good solution. Moreover, due to the intermittent features of the renewable energies, the S-MIC needs to have the ability to deliver power from each input source to the load, individually or simultaneously. Several S-MICs in table I and II can meet the requirements, except those composed with buck or boost and quasi-MICs. However, most of them have too many passive components or just simply sharing the output filter capacitor. Therefore, an S-MIC consists of a forward-
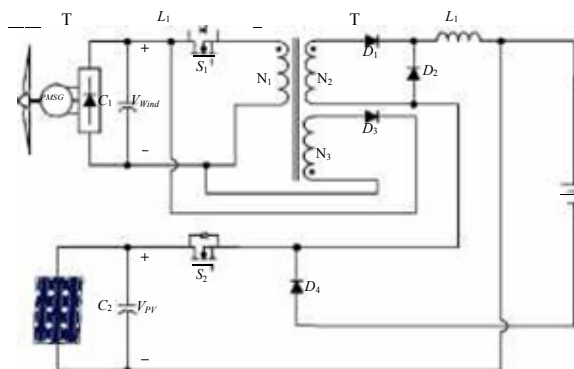
type I-PVSC and a buck-boost prime converter is proposed for the hybrid PV/wind power charger system to realize the MPPT function for each PV/wind source.

III. THE PROPOSED S-MIC FOR HYBRID PV/WIND BATTERY CHARGER

The schematic diagram of the proposed S-MIC for hybrid PV/Wind battery charger is shown in Fig. 10. The input voltage sources V_{PV} and V_{Wind} are the output terminals of the PV panel and the rectified output voltage of a wind turbine driven per manent magnet synchr onous generator (PMSG). By controlling the switches S_1 and S_2, both sources can achieve their maximum power with appropriate MPPT algorithm,

Fig. 10. The schematic diagram of the proposed S-MIC for hybrid PV/wind battery charger.

(a) Mode I

individually or simultaneously.

According to the status of the power switches, there are four different operation modes which can be explained as follows.

Mode I (S_1: On, S_2: On): The equivalent circuit for mode I is shown in Fig. 11(a) where both S_1 and S_2 are turned on, and D_2, D_3 and D_4 are turned off with reverse-biased voltages. In this operation mode, the input sources V_{Wind} and V_{PV} are connected in series to charge the energy storage component inductor L_1.

Mode II (S_1: On, S_2: Off): The equivalent circuit of mode II is shown in Fig. 11(b) where the power switch S_1 is turned on and S_2 is turned off. The diode D_2 and D_3 are reverse biased and can be treated as an open circuit. On the other hand, power switch S_2 for the input source V_{PV} is turned off and the power diode D_4 will provide a bypass path for inductor current i_{L1}. In this mode, the input source V_{Wind} will charge the energy storage component inductor L_1, as well as provide the electric energy for the battery.
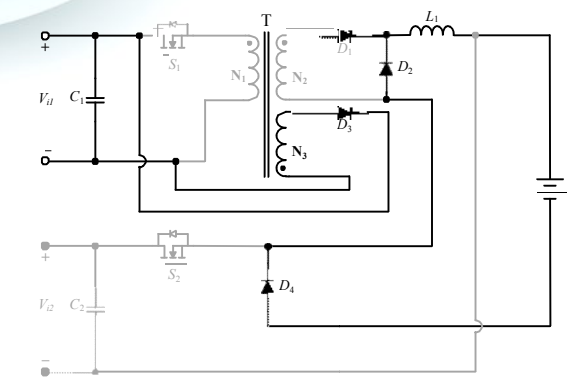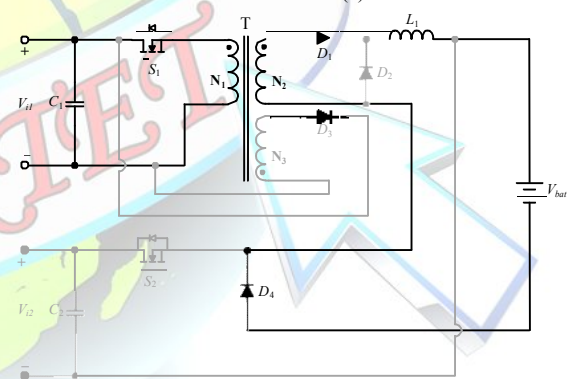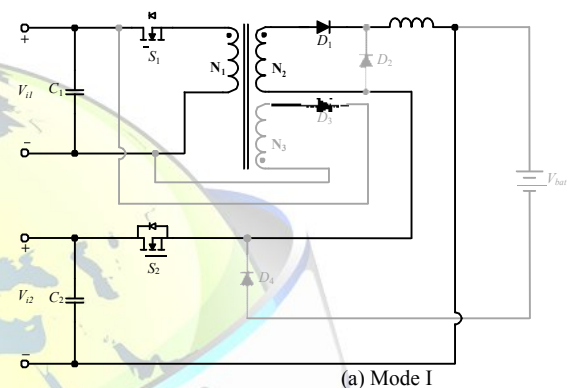
Mode III (S_1: Off, S_2: On): Fig. 11(c) shows the equivalent circuit for mode III. The power switch S_1 is turned off and S_2 is turned on. Also, the power diode D_1 and D_4 are reverse biased as open circuits, while D_2 and D_3 are forward biased as short circuits. In this operation mode, the transformer will be reset. The input source V_{PV} will charge the energy storage component inductor L_1.

Mode IV (S_1: Off, S_2: Off): The equivalent circuit for mode IV is shown in Fig. 11(d), with both S_1 and S_2 are turned off. Power diodes D_2 and D_4 will provide the current path for the inductor current. In this mode, the input sources V_{Wind} and V_{PV} are disconnected from the proposed double-input converter and

If $d_2 > d_1$, the equivalent operation circuit of the proposed converter in one switching cycle will follow another sequence of modes I, III, and IV. The same output voltage expression of (2) can be obtained. As shown in (2), if any one of the voltage sources is not available, i.e. either $d_1 = 0$ or $d_2 = 0$, the proposed S-MIC can still achieve the desired output voltage. Eq. (2) also reveals the advantage of the semi-isolated configuration under high voltage-transfer-ratio applications, since the power switches can be operated under moderate duty cycle with less current stress and higher efficiency.

It should be mentioned that both the S-MIC and the converters with parallel-connected configuration have their

pros and cons. For instance, the proposed S-MIC has larger conduction losses because of the series connected diodes and

transformer compared to two parallel-connected individual FB and BB converters. However, by saving the power losses from the reduced number of filter, auxiliary power source and peripheral circuit, the over-all efficiency of the S-MIC may be increased. Besides, the reduced size, weight, and cost are always the advantages of the S-MIC.

IV. THE SMALL SIGNAL AC MODEL

The voltage-current characteristic of the wind turbine driven PMSG is similar to the one of the PV panel. Therefore, under steady state, both the wind turbine and the PV panel can be represented, respectively, by a voltage source, V_{g1} or V_{g2}, in series with a resistor, R_{eq1} or R_{eq2}, whose value depends on the operating condition [27]-[29].

By using the state space averaging method [30], the small-signal ac model of the proposed hybrid PV/wind battery charger, as shown in Fig. 10, are represented in matrix form as:

$$\tilde{x} = A\tilde{x} + B\tilde{u}$$
$$\tilde{x} = \tilde{C}\tilde{x} + \tilde{D}\tilde{u} \tag{3}$$

where the state-variable x, input vector u, and output vector y, and parameter matrixes A B C D can be defined as:

$$[x] = [v_{Wind} \quad v_{PV} \quad i_{L1}]^T ;$$

$$[u] = [d_1 \quad d_2 \quad v_{bat}]^T ;$$

$$A = \begin{bmatrix} -\dfrac{1}{C_1 R_{eq1}} & 0 & -\dfrac{Nd_1}{C_1} \\ 0 & -\dfrac{1}{C_2 R_{eq2}} & -d_2 \\ \dfrac{Nd_1}{L_1} & \dfrac{d_2}{L_1} & 0 \end{bmatrix} ;$$

$$B = \begin{bmatrix} \dfrac{NI_{L1}}{C_1} & 0 & 0 \\ 0 & I_{L1} & 0 \\ -\dfrac{NV_{PV1}}{L_1} & -\dfrac{V_{PV2}+V_{bat}}{L_1} & \dfrac{d_2-1}{L_1} \end{bmatrix} ;$$

$$\begin{bmatrix} 1 & 0 & 0 \end{bmatrix}$$

The small-signal ac model transfer function matrix G of the converter can be obtained as:

$$G = C(sI - A)^{-1} B + D \tag{5}$$

where I is the identity matrix.

According to the number of control variables and (5), the relationship of the transfer function matrix are obtained as follows:

$$\begin{bmatrix} v_{Wind} \\ v_{PV} \\ y \end{bmatrix} = \begin{bmatrix} G_{11} & G_{12} & G_{13} \\ G_{21} & G_{22} & G_{23} \\ & G & \end{bmatrix} \begin{bmatrix} d_1 \\ d_2 \\ v_{bat} \\ u \end{bmatrix} \tag{6}$$

where component G_{ij} represents the transfer function between y_i and u_j. Table IV lists the derived open-loop control-to-input transfer functions of the S-MIC with appropriate approximation. The derived transfer functions and parameters in Table IV are the key components in the control loop and are the foundation of controller design.

V. CONTROLLER DESIGN

In order to improve the frequency response of the system and achieve desired MPPT performance with input voltage regulation, an appropriate designed compensator based on the transfer function developed in the previous section is necessary. The control-to-input voltage transfer functions are the key components of the loop gain and have a significant effect on regulator performance, which further relates to the MPPT performance. However, due to the interaction between the two control loops, the design of the compensators is no longer as straight-forward as it used to be for a single input converter. Fig. 12 shows the control block diagram of the proposed S-MIC, where the closed loop control-to-input transfer functions can be derived using Mason's gain formula [31], and the expression of the two loop gains, $T_X(s)$ and $T_Y(s)$, measured at the designated location are shown in (12) and (13). The results show that, if $T_X(s)$ and $T_Y(s)$ are both larger than unity, which can be achieved easily with proper design before the crossover frequency, the complexity can be reduced and the decoupled control-to-input transfer functions $G_1(s)$ and $G_2(s)$ can be obtained.
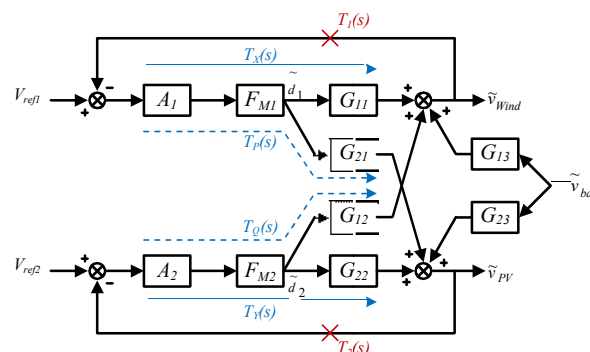
TABLE IV
THE OPEN-LOOP CONTROL-TO-INPUT TRANSFER FUNCTIONS.

Open-loop control-to-input transfer functions

$$G_{11}(s) = \frac{\tilde{v}_{Wind}}{\tilde{d}_1} \approx - \frac{C_m \cdot N \cdot R_{eqm} \cdot (I_{L1} \cdot R_{eq2}^2 \cdot d_2 + d_1 \cdot N \cdot V_{Wind}) \cdot \left(1 + \frac{s}{\omega_{z1}}\right) \cdot \left(1 + \frac{s}{\omega_{z2}}\right)}{R_{eq2} \cdot (C_2 \cdot d_1^2 \cdot N^2 + C_1 \cdot d_2^2) \cdot \Delta(s)} \tag{7}$$

$$G_{12}(s) = \frac{\tilde{v}_{Wind}}{\tilde{d}_2} \approx - \frac{C_m \cdot d_1 \cdot N \cdot R_{eqm} \cdot (V_{PV} + V_{bat} - d_2 \cdot I_{L1} \cdot R_{eq2}) \cdot \left(1 + \frac{s}{\omega_{z3}}\right)}{R_{eq2} \cdot (C_2 \cdot d_1^2 \cdot N^2 + C_1 \cdot d_2^2) \cdot \Delta(s)} \tag{8}$$

$$G_{21}(s) = \frac{\tilde{v}_{PV}}{\tilde{d}_1} \approx - \frac{C_m \cdot d_2 \cdot N \cdot R_{eqm} \cdot (V_{Wind} - d_1 \cdot N \cdot I_{L1} \cdot R_{eq1}) \cdot \left(1 + \frac{s}{\omega_{z4}}\right)}{R_{eq1} \cdot (C_2 \cdot d_1^2 \cdot N^2 + C_1 \cdot d_2^2) \cdot \Delta(s)} \tag{9}$$

$$G_{22}(s) = \frac{\tilde{v}_{PV}}{\tilde{d}_2} \approx - \frac{C_m \cdot R_{eqm} \cdot (I_{L1} \cdot R_{eq1}^2 \cdot d_1^2 \cdot N + d_2 \cdot (V_{PV} + V_{bat})) \cdot \left(1 + \frac{s}{\omega_{z5}}\right) \cdot \left(1 + \frac{s}{\omega_{z6}}\right)}{R_{eq1} \cdot (C_2 \cdot d_1^2 \cdot N^2 + C_1 \cdot d_2^2) \cdot \Delta(s)} \tag{10}$$

Parameters

$$\omega_{z1} = \frac{1}{C_2 \cdot R_{eq2}} + \frac{d_2^2 \cdot I_{L1} \cdot R_{eq2}}{C_2 \cdot d_1 \cdot N \cdot R_{eq2} \cdot V_{Wind} - I_{L1} \cdot L_1} \; ; \; \omega_{z2} = \frac{d_1 \cdot N \cdot V_{Wind}}{I_{L1} \cdot L_1} - \frac{d_2 \cdot I_{L1}^2 \cdot R_{eq2}}{C_2 \cdot d_1 \cdot N \cdot R_{eq2} \cdot V_{Wind} - I_{L1} \cdot L_1} \; ;$$

$$\omega_{z3} = \frac{1}{C_2 \cdot R_{eq2}} - \frac{d_2 \cdot I_{L1} \cdot R_{eq2}}{C_2 \cdot R_{eq2} \cdot (V_{PV} + V_{bat})} \; ; \; \omega_{z4} = \frac{1}{C_1 \cdot R_{eq1}} - \frac{d_1 \cdot N \cdot I_{L1} \cdot R_{eq1}}{C_1 \cdot R_{eq1} \cdot V_{Wind}} \; ;$$

$$\omega_{z5} = \frac{1}{C_1 \cdot R_{eq1}} + \frac{d_1^2 \cdot N^2 \cdot I_{L1} \cdot R_{eq1}}{C_1 \cdot d_2 \cdot R_{eq1} \cdot (V_{PV} + V_{bat}) - I_{L1} \cdot L_1} \; ; \; \omega_{z6} = \frac{d_2 \cdot (V_{PV} + V_{bat})}{I_{L1} \cdot L_1} - \frac{d_1 \cdot N^2 \cdot I_{L1}^2 \cdot R_{eq1}}{C_1 \cdot d_2 \cdot R_{eq1} \cdot (V_{PV} + V_{bat}) - I_{L1} \cdot L_1} \; ;$$

$$\Delta(s) = \left(1 + \frac{s}{\omega_{p1}}\right) \cdot \left[1 + \frac{s}{Q \omega_0} + \left(\frac{s}{\omega_0}\right)^2\right] \; ;$$

$$\omega_{p1} = \frac{1}{C_m \cdot R_{eqm}} \; ; \; \omega_0 = \sqrt{\frac{d_2^2}{C_2 \cdot L_1} + \frac{d_1^2 \cdot N^2}{C_1 \cdot L_1}} \; ; \; Q = C_n R_{eqn} \sqrt{\frac{d_2^2}{C_2 \cdot L_1} + \frac{d_1^2 \cdot N^2}{C_1 \cdot L_1}} \; . \tag{11}$$

$$m : n = \begin{cases} 1 : 2 & if \; d_1 \cdot N < d_2 \\ 2 : 1 & if \; d_1 \cdot N > d_2 \end{cases}$$

$$T_1(s) = T_X(s) - \frac{T_P(s) \cdot T_Q(s)}{1 + T_Y(s)}$$
$$\approx \underbrace{\left(G_{11} - \frac{G_{12} \cdot G_1}{G_{22}}\right)}_{G_1} \cdot F_{M1} \cdot A_1(s) \tag{12}$$

$$T_2(s) = T_Y(s) - \frac{T_P(s) \cdot T_Q(s)}{1 + T_X(s)}$$
$$\approx \underbrace{\left(G_{22} - \frac{G_{12} \cdot G_{21}}{G_{11}}\right)}_{G_2} \cdot F_{M2} \cdot A_2(s) \tag{13}$$

$$G_1(s) = -K_1 \cdot \frac{\left(1 + \frac{s}{\omega_{z7}}\right)}{\left(1 + \frac{s}{\omega_{p2}}\right) \cdot \left(1 + \frac{s}{\omega_{p3}}\right)} \tag{14}$$

$$G_2(s) = -K_2 \cdot \frac{\left(1 + \frac{s}{\omega_{z7}}\right)}{\left(1 + \frac{s}{\omega_{p4}}\right) \cdot \left(1 + \frac{s}{\omega_{p5}}\right)} \tag{15}$$

where

From (12) and (13), and the control-to-input transfer functions listed in Table IV. The transfer functions of $G_1(s)$ and $G_2(s)$ can be derived as:

$$K_1 = \frac{I_{L1} \cdot N \cdot R_{eq1} \cdot [d_1 \cdot N \cdot V_{Wind} + d_2 \cdot (V_{PV} + V_{bat})]}{I_{L1} \cdot R_{eq1} \cdot d_1^2 \cdot N^2 + d_2 \cdot (V_{PV} + V_{bat})} \; ;$$

$$K_2 = \frac{I_{L1} \cdot R_{eq\,2} \cdot [d_1 \cdot N \cdot V_{Wind} + d_2 \cdot (V_{PV} + V_{bat})]}{I_{L1} \cdot R_{eq\,2} \cdot d_2^2 + d_1 \cdot N \cdot V_{Wind}};$$

$$\omega_{z7} = \frac{d_2 \cdot (V_{PV} + V_{bat})}{I_{L1} \cdot L_1} + \frac{d_1 \cdot N \cdot V_{Wind}}{I_{L1} \cdot L_1};$$

$$\omega_{p2} = \omega_{z5}; \quad \omega_{p3} = \omega_{z6}; \quad \omega_{p4} = \omega_{z1}; \quad \omega_{p5} = \omega_{z2}. \quad (16)$$

Equation (14) and (15) show the decoupled control-to-input transfer functions, $G_1(s)$ and $G_2(s)$. One important difference, compared to the open loop control-to-input transfer functions $G_{11}(s)$ in (7) and $G_{22}(s)$ in (10), is that the high quality factor double pole with sharp phase change at the corner frequency is divided into two single, well-separated low quality factor poles. Therefore, the phase change of (14) and (15) will be smoother than those of (7) and (10) and the system stability can be easily achieved with proper controller design. However, due to the intermittent features of the renewable energies, the S-MIC will deliver power from each input source to the load either individually or simultaneously. Therefore, the compensator designed for each control loop has to be stable for both the decoupled control-to-input transfer function and the corresponding forward or buck-boost control-to-input transfer function, respectively.

By setting some parameters in (7) equal to zero, those who are not included in a forward converter such as the duty ratio d_2, the capacitor C_2 and the resistor R_{eq2}, the control-to-input transfer function of the forward converter $G_{df}(s)$ can be derived as:

$$G_{df}(s) = G_{11}(s) \Big|_{\substack{d_2=0 \\ C_2=0 \\ R_{eq\,2}=0}}$$

$$= -\frac{V_{Wind}}{d_1} \cdot \frac{\left(1 + \dfrac{s}{\omega_{z8}}\right)}{1 + \dfrac{s}{Q_f \cdot \omega_{0f}} + \left(\dfrac{s}{\omega_{0f}}\right)^2} \quad (17)$$

where

$$\omega_{0f} = \frac{d_1 \cdot N}{\sqrt{L_1 \cdot C_1}}; \quad Q_f = C_1 \cdot R_{eq1} \cdot \frac{d_1 \cdot N}{\sqrt{L_1 \cdot C_1}};$$

$$\omega_{z8} = \frac{d_1 \cdot N \cdot V_{Wind}}{I_{L1} \cdot L_1}. \quad (18)$$

Similarly, the control-to-input transfer functions of the buck-boost converter $G_{db}(s)$ can be derived from (10) as:

$$G_{db}(s) = G_{22}(s) \Big|_{\substack{d_1=0 \\ C_1=0 \\ R_{eq\,1}=0 \\ N=0}}$$

$$= -\frac{V_{PV} + V_{bat}}{d_2} \cdot \frac{\left(1 + \dfrac{s}{\omega_{}}\right)}{1 + \dfrac{s}{Q_b \cdot \omega_{0b}} + \dfrac{s}{}} \quad (19)$$

where

$$\omega_{0b} = \frac{d_2}{\sqrt{L_1 \cdot C_2}}; \quad Q_b = C_2 \cdot R_{eq2} \cdot \frac{d_2}{\sqrt{L_1 \cdot C_2}},$$

$$\omega_{z9} = \frac{d_2 \cdot (V_{PV} + V_{bat})}{I_{L1} \cdot L_1}. \quad (20)$$

By examining (14) and (17), a type-III compensator with two zeros and three poles and the ability to stabilize the system in all modes is introduced to the control loop of the wind turbine. For the proposed S-MIC applications, the quantities of the inductance and the capacitance are within the order of micro-henry or micro-farad. With the practical circuit parameters quantities, it can be observed that the denominator of ω_{0f} is smaller than the denominator of ω_{p2} and ω_{p3} while the numerator of ω_{0f} is at the same level to the numerator of ω_{p2} and much smaller than the numerator of ω_{p3}. Therefore, the angular frequency ω_{0f} will be larger than ω_{p2} but smaller than ω_{p3}. Hence, by placing the two zeros on ω_{p2} and ω_{p3}, the double poles at ω_{0f} will also be surrounded and the excessive phase lag can be reduced. However, if ω_{p2} or ω_{p3} is too far apart the zeros can also be placed closer to ω_{0f} without affecting the stability. Then, one pole is placed at the origin to increase the magnitude of the loop gain at low frequency, another pole is placed on ω_{z8} to cancel out the effect of the zero, and the last pole is used to attenuate the switching noise. Similar results can be discovered for the control loop of the PV by examining (15) and (19) with the same procedure.

VI. COMPUTER SIMULATIONS AND EXPERIMENTAL RESULTS

To verify the feasibility and performance of the proposed S-MIC for the hybrid PV/Wind power charger system, both computer simulations and hardware experiments with specifications listed in Table V are carried out. The circuit simulation software PSIM is adopted to obtain the simulated behavior of the proposed S-MIC. The software MATLAB is adopted to draw the Bode plots of those data obtained from the derived mathematical equations, computer simulations, and hardware measurements.

In order to testify the validity of the derived decoupled control-to-input transfer functions shown in (14) and (15), two different compensators $A_1(s)$ and $A_2(s)$, based on the controller design criterion proposed in the previous section, with crossover frequency at 1 *kHz*, are designed as:

TABLE V
THE SPECIFICATIONS FOR BOTH SIMULATION AND EXPERIMENT

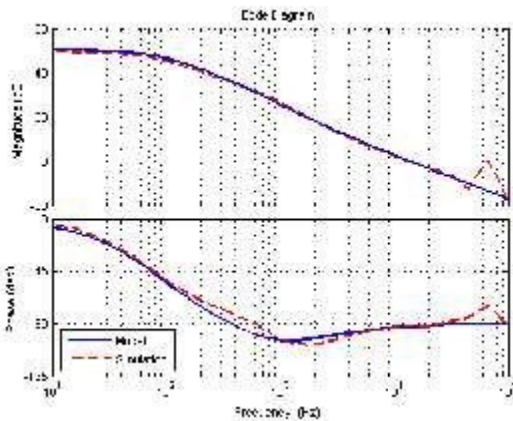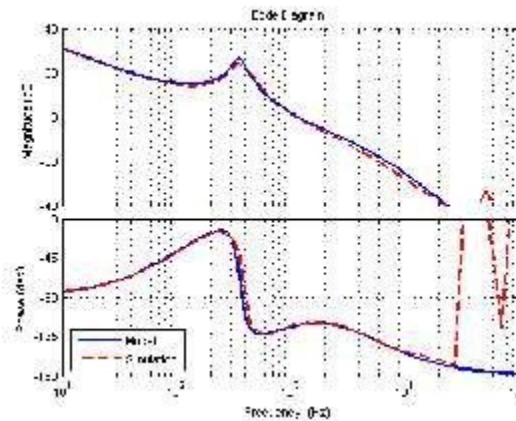| Symbol	Meaning	Value
$V_{PV,mpp}$	MPP voltage of PV	35V
$I_{PV,mpp}$	MPP current of PV	3.33A
$V_{wind,mpp}$	Rectified MPP voltage of wind turbine	75V
$I_{wind,mpp}$	Rectified MPP current of wind turbine	2A
V_{bat}	Battery voltage	24V
L_1	Output inductor	200μH
C_1	Input capacitor	100μF

Fig. 13. The bode plot of G_1.

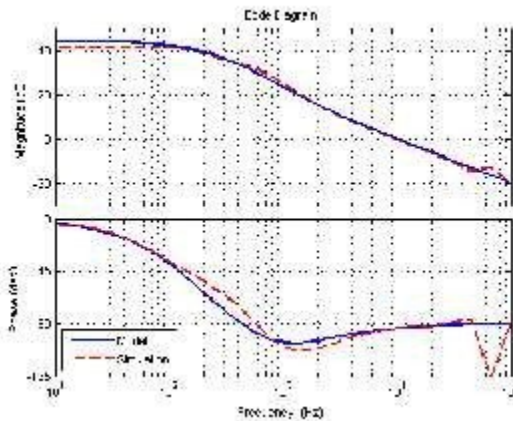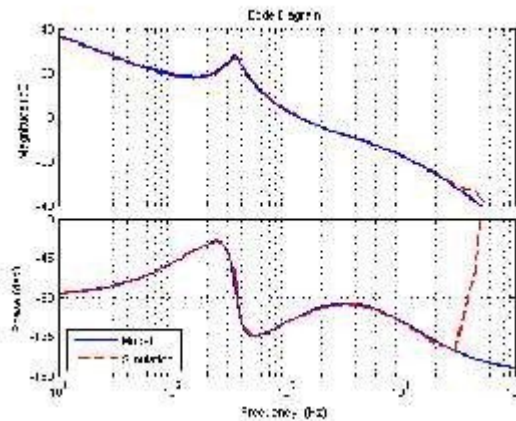Fig. 15. The bode plot of T_f.

Fig. 14. The bode plot of G_2.

Fig. 16. The bode plot of T_b.

$$A_1(s) = \frac{1.0\,e^7 s^2 + 3.77\,e^{10} s + 1.97\,e^{13}}{34.6\,s^3 + 1.4\,e^6 s^2 + 9.87\,e^9 s}$$

$$A_2(s) = \frac{3.5e^5 s^2 + 1.65\,e^9 s + 1.24\,e^{12}}{3.11\,s^3 + 1.26\,e^5 s^2 + 8.88\,e^8 s} \qquad (21)$$

Fig. 13 and Fig. 14 show the frequency responses of $G_1(s)$ and $G_2(s)$, where both magnitude and phase curves of the transfer function obtained from the mathematical model and PSIM simulation are shown on the same chart. Since the state space averaging models are accurate only up to the half of the switching frequency, the frequency response of the derived mathematical models are found to be coincided with the simulated ones up to tens of *kHz*.

After testifying the validity of the derived decoupled control-to-input transfer functions, the stability of the S-MIC under pure forward and buck-boost operation has to be confirmed. Fig. 15 and Fig. 16 show the frequency responses of the loop gains T_f and T_b, where the corresponding control-to-input transfer functions $G_{df}(s)$ and $G_{db}(s)$ are compensated by the compensator $A_1(s)$ and $A_2(s)$, respectively. The results show that the S-MIC will be stable under pure forward and buck-boost operation, since the phase margins are both greater than 45 degrees.

A hardware prototype with the same circuit parameters and

the accuracy of the small-signal model and the performance of the proposed S-MIC. The PV simulator, Agilent E4360A, is used to simulate both the rectified wind turbine and the PV panel. The MPPT function and the compensator are realized by controller used for simulation has been built and tested to verify a digital controller dsPIC33FJ16GS502. Fig. 17 and Fig. 18 show the comparisons between the simulation loop gain, experimental loop gain, and the loop gain derived from small-signal ac model. Due to the digital control loop time delay resulting from analog to digital conversion, computation and so on, the time delay of switching converters is usually equal to one switching cycle [32], [33]. The model with the time delay effect considered by the Padé-approximation is added in the comparison. It should be mentioned that the experiment bode plots of the prototype circuit are obtained by using the frequency response analyzer AP-300. The results validate the accuracy of the developed small-signal ac model since its bode plot coincides with the simulation and digital hardware experiment results for up to almost half of the switching frequency. Fig. 17 and 18 also show that the S-MIC is stable with the controller obtained by the proposed design criteria since the phase margins are greater than 45 degrees.
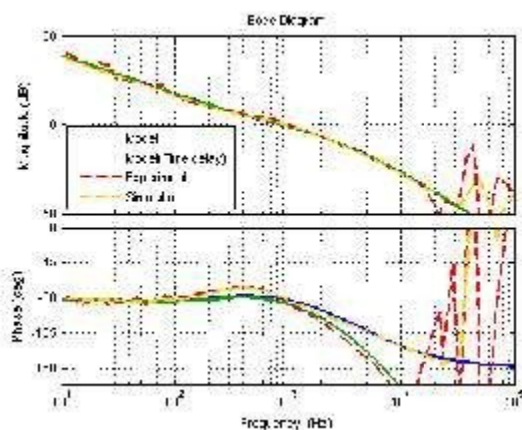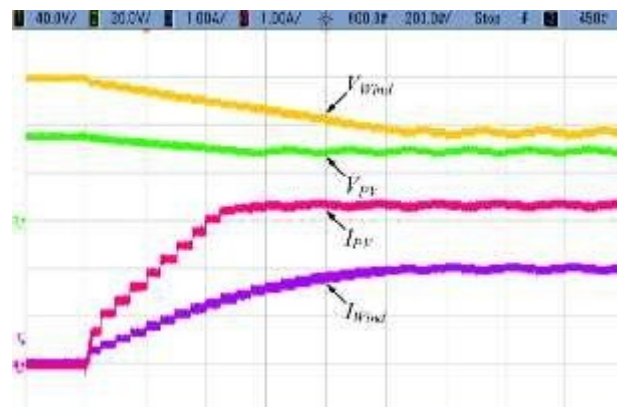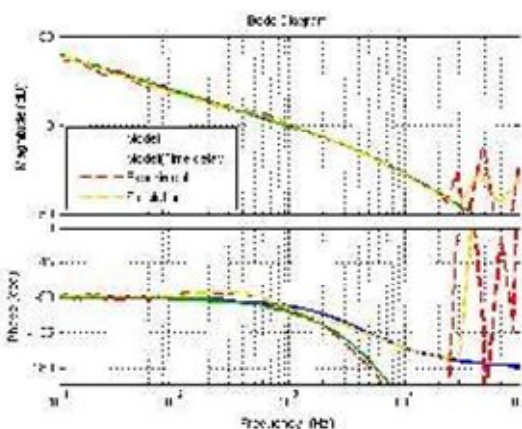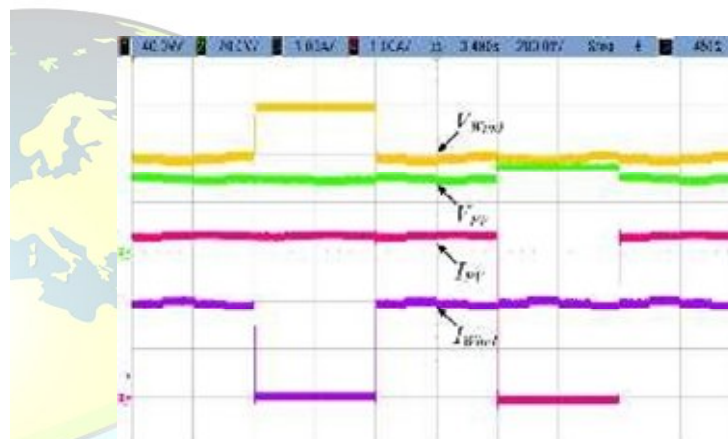
Fig. 17. The bode plot of T_1.

Fig. 19. The MPPT feature for both PV module and Wind turbine.

Fig. 18. The bode plot of T_2. Fig.

20. Sudden power off-on changes of the wind turbine and the PV module.

battery simultaneously and achieve their maximum power point without affecting each other.

It is well-known that the renewable energy has an intermittent feature. Therefore, to verify the transient response of the proposed S-MIC with the ability to deliver power to the battery either individually or simultaneously, the input voltage of the PV module or the wind turbine will be forced to turn off for a period of time then resume on afterward.

Fig. 20 shows the measured input voltages and current when the wind turbine and the PV module has sudden power off-on changes, respectively. It can be clearly seen that the operation of the other input source, is not affected by the sudden change of the wind power or the PV module. It also reveals that the proposed S-MIC can transfer power from two different sources either simultaneously or individually, without affecting each other's operation. The experimental results verify the performance of the controller for the proposed S-MIC.

VII. CONCLUSION

In this paper, four I-PVSCs and three I-PCSC are developed based on the circuit structure of five basic isolated dc-dc converters. A systematic approach to synthesize the MIC family and the combinations of the S-MIC and I-MIC series are presented. A S-MIC for hybrid PV/wind power charger system, which can simplify the power system, reduce the cost, deliver continuous power and overcome the high voltage-transfer-ratio problem has been proposed. The operation principle of the proposed S-MIC, formed by a forward-type PVSC and a buck-boost prime converter, has been introduced. The small signal ac model of the proposed S-MIC has been derived and the controller design has been developed. Computer simulations and prototype hardware circuit experimental results are presented to verify the accuracy of the proposed small signal model and the performance of controller for the proposed S-MIC for hybrid PV/wind battery charger system.

REFERENCES

[1] Q. Li and P. Wolfs, "A review of the single phase photovoltaic module integrated converter topologies with three different DC link configurations," *IEEE Trans. Power Electron.*, vol.23, no.3, pp.1320-1333, May 2008.

[2] S.M. Muyeen, R. Takahashi, T. Murata, and J. Tamura, "A variable speed wind turbine control strategy to meet wind farm grid code requirements," *IEEE Trans. Power Electron.*, vol.25, no.1, pp.331-340, Feb. 2010.

[3] X. Li and A.K.S. Bhat, "Analysis and design of high-frequency isolated dual-bridge series resonant DC/DC Converter," *IEEE Trans. Power Electron.*, vol.25, no.4, pp.850-862, April 2010.

[4] Y.-M. Chen, Y.-C. Liu, and F.-Y. Wu, "Multi-input DC/DC converter based on the multiwinding transformer for renewable energy applications," *IEEE Trans. Ind. Appl.*, vol.38, no.4, pp.1096-1104, Jul/Aug 2002.[5] Y.-M. Chen, Y.-C. Liu, and F.-Y. Wu, "Multiinput converter with power factor correction, maximum power point tracking, and ripple-free input currents," *IEEE Trans. Power Electron.*, vol.19, no.3, pp. 631- 639, May 2004.

[6] J. Cao and A. Emadi, "A New Battery/UltraCapacitor Hybrid Energy Storage System for Electric, Hybrid, and Plug-In Hybrid Electric Vehicles," *IEEE Trans. Power Electron.*, vol. 27, no. 1, pp. 122-132, Jan. 2012.

[7] N. Benavides and P. Chapman, "Object oriented modeling of a multiple-input multiple-output flyback converter in dymola," *IEEE Workshop on Computers in Power Electronics*, pp.156-160, 2004.

[8] Z. Ding, C. Yang, Z. Zhang, C. Wang, and S. Xie "A Novel Soft-Switching Multiport Bidirectional DC-DC Converter for Hybrid Energy Storage Systems," *IEEE Trans. Power Electron.*, vol. 29, no. 4, pp. 1595-1609, April 2014.

[9] S. Danyali, S.H. Hosseini, and G.B. Gharehpetian, "New Extendable Single-Stage Multi-input DC-DC/AC Boost Converter," *IEEE Trans. Power Electron.*, vol. 29, no. 2, pp. 775-788, Feb. 2014.

[10] H. Matsuo, W. Lin, F. Kurokawa, T. Shigemizu, and N. Watanabe, "Characteristics of the multi-input dc-dc converter," *IEEE Trans. Industrial Electronics*, vol.51, no.3, pp.625-631, June 2004.

[11] Y.-M. Chen, Y.-C. Liu, and S.-H. Lin, "Double-input PWM DC/DC converter for high-/low-voltage sources," *IEEE Trans. Industrial Electronics,* vol.53, no.5, pp.1538-1545, Oct. 2006.

[12] H. Tao, A. Kotsopoulos, J. L. Duarte, and M. A. M. Hendrix, "Family of multiport bidirectional dc-dc converters," *IEE Proc. Electron. Power Appl.,* vol. 153, no. 3, pp. 451-458, May 2006.

[13] R. Zhao and A. Kwasinski, "Multiple-input single ended primary inductor converter (SEPIC) converter for distributed generation applications," in *Proc. IEEE Energy Convers. Congr. Expo.*, 2009, pp.1847-1854.

[14] A. Kwasinski, "Identification of feasible topologies for multiple-input DC–DC converters," *IEEE Trans. Power Electron.*, vol.24, no.3, pp.856-861, March 2009.

[15] A. Khaligh, J. Cao, and Y.-J. Lee, "A multiple-input DC–DC converter topology," *IEEE Trans. Power Electron.*, vol.24, no.3, pp.862-868, March 2009.

[16] C. Zhao, S.D. Round, and J.W. Kolar, "An isolated three-port bidirectional DC-DC converter with decoupled power flow management," *IEEE Trans. Power Electron.*, vol.23, no.5, pp.2443-2453, Sep. 2008.

[17] H. Tao, J.L. Duarte, and M.A.M. Hendrix, "Three-port triple-half-bridge bidirectional converter with zero-voltage switching," *IEEE Trans. Power Electron.*, vol.23, no.2, pp.782-792, March 2008.

[18] S.-Y. Yu and A. Kwasinski, "Analysis of Soft-Switching Isolated Time-Sharing Multiple-Input Converters for DC Distribution Systems," Power Electronics, *IEEE Trans. Power Electron.*, vol. 28, no. 4, pp. 1783-1794, April 2013.

[19] F. Liu, Z. Wang, Y. Mao, and X. Ruan, "Asymmetrical Half-Bridge Double-Input DC/DC Converters Adopting Pulsating Voltage Source Cells for Low Power Applications," *IEEE Trans. Power Electron.*, vol. 29, no. 9, pp. 4741-4751, Sept.2014.

[20] Y.-C. Liu and Y.-M. Chen, "A Systematic Approach to Synthesizing Multi-Input DC-DC Converters," *IEEE Trans. Power Electron.*, vol. 24, pp. 116-127, Jan. 2009.

[21] M. Veerachary, "Two-Loop Controlled Buck–SEPIC Converter for Input Source Power Management," *IEEE Trans. Industrial Electronics*, vol. 59, no.11, pp. 4075-4087, Nov.2012.

[22] Z. Qian, O. Abdel-Rahman, and I. Batarseh, "An integrated four-port DC/DC converter for renewable energy applications," *IEEE Trans. Power Electron.*, vol.25, no.7, pp.1877-1887, July 2010.

[23] Z. Qian, O. Abdel-Rahman, H. Al-Atrash, and I. Batarseh, "Modeling and control of three-port DC/DC converter interface for satellite applications," *IEEE Trans. Power Electron.*, vol.25, no.3, pp.637-649, March 2010.

[24] F. Nejabatkhah, S. Danyali, S.H. Hosseini, M. Sabahi, and S.M. Niapour, "Modeling and Control of a New Three-Input DC–DC Boost Converter for Hybrid PV/FC/Battery Power System," *IEEE Trans. Power Electron.*, vol.27, no.5, pp.2309-2324, May 2012.

[25] R. Ahmadi, H. Zargarzadeh, and M. Ferdowsi, "Nonlinear Power Sharing Controller for a Double-Input H-Bridge-Based Buckboost–Buckboost Converter," *IEEE Trans. Power Electron.*, vol. 28, no. 5, pp. 2402-2414, May 2013.

[26] I. Batarseh, *Power Electronic Circuits*, John Wiley & Sons, 2004.

[27] N. Femia, G. Petrone, G. Spagnuolo, and M. Vitelli, "Optimization of perturb and observe maximum power point tracking method," *IEEE Trans. Power Electron.*, vol.20, no.4, pp. 963- 973, July 2005.

[28] W. Xiao, W. G. Dunford, P. R. Palmer, and A. Capel, "Regulation of photovoltaic voltage," *IEEE Trans. Ind. Electron.*, vol. 54, no. 3, pp. 1365-1374, Jun. 2007.

[29] C.-W. Chen, K.-H. Chen, and Y.-M. Chen, "Modeling and Controller Design of an Autonomous PV module for DMPPT PV Systems," *IEEE Trans. Power Electron.*, vol. 29, no. 9, pp. 4723-4732, Sept. 2014.

[30] R. W. Erickson and D. Maksimović, *Fundamental of Power Electronics*, 2nd ed. Norwell, MA, USA: Kluwer, 2001.

[31] S. J. Mason, "Feedback theory-further properties of signal flow graphs," in *Proc. IRE*, vol. 44, no. 7, pp. 920-926, July 1956.

[32] S. Bibian and H. Jin, "Time delay compensation of digital control for DC switchmode power supplies using prediction techniques," *IEEE Trans. Power Electron.*, vol.15, no.5, pp. 835-842, Sept. 2000.

[33] J. Chen, A. Prodic, R. W. Erickson, and D. Maksimovic, "Predictive digital current programmed control," *IEEE Trans. Power Electron.*, vol.18, no.1, pp. 411-419, Jan. 2003.